Phosphate graphene as an intrinsically osteoinductive scaffold for stem cell-driven bone regeneration

Anne M. Arnold[a], Brian D. Holt[a], Leila Daneshmandi[b,c,d,e], Cato T. Laurencin[b,c,d,e,f,g,1], and Stefanie A. Sydlik[a,h,1]

[a]Department of Chemistry, Carnegie Mellon University, Pittsburgh, PA 15213; [b]Connecticut Convergence Institute for Translation in Regenerative Engineering, UConn Health, Farmington, CT 06030; [c]Raymond and Beverly Sackler Center for Biological, Physical and Engineering Sciences, UConn Health, Farmington, CT 06030; [d]Department of Biomedical Engineering, University of Connecticut, Storrs, CT 06269; [e]Department of Orthopaedic Surgery, UConn Health, Farmington, CT 06030; [f]Department of Material Science and Engineering, University of Connecticut, Storrs, CT 06269; [g]Department of Chemical and Biomolecular Engineering, University of Connecticut, Storrs, CT 06269; and [h]Department of Biomedical Engineering, Carnegie Mellon University, Pittsburgh, PA 15213

Edited by Phillip Messersmith, University of California, Berkeley, CA, and accepted by Editorial Board Member John A. Rogers January 22, 2019 (received for review September 14, 2018)

Synthetic, resorbable scaffolds for bone regeneration have potential to transform the clinical standard of care. Here, we demonstrate that functional graphenic materials (FGMs) could serve as an osteoinductive scaffold: recruiting native cells to the site of injury and promoting differentiation into bone cells. By invoking a Lewis acid-catalyzed Arbuzov reaction, we are able to functionalize graphene oxide (GO) to produce phosphate graphenes (PGs) with unprecedented control of functional group density, mechanical properties, and counterion identity. In aqueous environments, PGs release inducerons, including Ca^{2+} and PO_4^{3-}. Calcium phosphate graphene (CaPG) intrinsically induces osteogenesis in vitro and in the presence of bone marrow stromal cells (BMSCs), can induce ectopic bone formation in vivo. Additionally, an FGM can be made by noncovalently loading GO with the growth factor recombinant human bone morphogenetic protein 2 (rhBMP-2), producing a scaffold that induces ectopic bone formation with or without BMSCs. The FGMs reported here are intrinsically inductive scaffolds with significant potential to revolutionize the regeneration of bone.

graphene | stem cells | bone | biomimetic

Strong, biodegradable, and intrinsically osteoinductive implants have the capacity to revolutionize the treatment of severe bone injuries. Despite their potential, decades of research have failed to generate a synthetic material that incorporates all of the necessary characteristics of an ideal bone scaffold and cultivates an optimal environment for bone regeneration. Current treatments rely on surgical fixation of bone grafts or devices to impart structural stability at the site of injury. However, these therapies suffer limitations: suitable donor sites are at a premium for autografts, while allografts risk rejection. Metallic hardware produces good results but remains permanently (1, 2), which limits use in children and can damage surrounding tissue (3). Regenerative engineering strategies could ultimately produce superior degradable scaffolds that activate the body's innate healing pathways and eliminate the need for grafts and nonresorbable prosthetics.

Bone spontaneously heals minor fractures; however, inherent healing mechanisms fail when tissue is severely damaged (4). To enhance the natural regenerative response, stem cell therapies hold tremendous potential (5), but the recruitment, retention, and differentiation of these cells at the site of injury remain a challenge (6, 7). To support cell-mediated regeneration, a resorbable synthetic scaffold that matches the chemical and mechanical properties of bone and retains and drives differentiation of stem cells could substantially improve the treatment of traumatic bone injuries. However, no synthetic scaffold material has been reported that provides mechanical stabilization, degradability, and cell instructive moieties.

To drive regenerative healing, a composite material that mimics the complexities of native tissue must be developed. One promising composite component is graphene oxide (GO), a nanostructured carbon material with mechanical strength (8), an aqueous degradation pathway (9), and tunable surface chemistry (10). Furthermore, cells readily adhere to and grow on graphenic materials (11), and GO offers a plethora of organic functionalities that can be exploited to derive functional graphenic materials (FGMs) (12). However, many reported functionalization strategies for creating FGMs lack the control and nuance required for biomimetic functionalization.

Herein, we report phosphate graphene (PG) as a biomimetic class of stem cell scaffolds for bone regeneration that show intrinsic osteoinductivity in vitro and in vivo. To produce this scaffold material, the Arbuzov reaction was borrowed from organic chemistry and applied to GO: by using a Lewis acid catalyst, reaction conditions allow for unprecedented control of PG composition, enabling the production of hydroxyapatite-like surfaces. Furthermore, this chemistry incorporates selectively labile bonds to enable the tunable, controlled release of "inducerons": (13) ions that are known to direct osteogenic differentiation of stem cells without the use of growth factors. This material exhibits tunable mechanical properties and degradability and retains stem cells while instructing their osteogenic differentiation. Thus, PG is a promising scaffold material that could enable stem cell-driven bone regeneration.

Rationale for Material Design

The ideal scaffold for stem cell-driven bone regeneration encourages stem cell retention and differentiation, is mechanically sound and intrinsically ordered to support activity while the

Significance

Traumatic bone injuries or deformities are among the most common conditions that require surgical intervention affecting patients in the United States today. Current treatment options suffer shortcomings, clearly demonstrating a clinical need for tissue replacement techniques. An ideal treatment consists of a scaffold that promotes regeneration, matches the chemical and mechanical properties of bone, and degrades with a timeline matching the healing process. However, this ideal scaffold has not been realized. Here, we present a degradable, graphene-based material that mimics the chemical and mechanical composition of bone, promotes differentiation of stem cells, and leads to the formation of new bone in an animal model.

Author contributions: C.T.L. and S.A.S. designed research; A.M.A., B.D.H., and L.D. performed research; A.M.A., B.D.H., L.D., C.T.L., and S.A.S. analyzed data; and A.M.A., B.D.H., L.D., C.T.L., and S.A.S. wrote the paper.

Conflict of interest statement: Carnegie Mellon University has filed a patent application on behalf of the inventors (A.M.A., B.D.H., L.D., C.T.L., and S.A.S.) entitled phosphate functionalized graphene oxide-based bone scaffolds.

This article is a PNAS Direct Submission. P.M. is a guest editor invited by the Editorial Board.

[1]To whom correspondence may be addressed. Email: laurencin@uchc.edu or ssydlik@andrew.cmu.edu.

This article contains supporting information online at www.pnas.org/lookup/suppl/doi:10.1073/pnas.1815434116/-/DCSupplemental.

Published online February 22, 2019.

injury is healing, and degrades over a year to match the timeline of intrinsic bone healing. FGMs chemically derived from GO have an aqueous degradation pathway, intrinsic long-range order, and robust mechanical properties. Furthermore, recent research has shown GO to be compatible, support cell adhesion, and in some cases, promote osteogenic differentiation of stem cells. Here, we describe a method to create an osteomimetic PG scaffold. This synthetic approach gives us a graphenic scaffold with hydroxyapatite-like functionality at the interface and furthermore, is programmed to elute osteoinstructive inducerons, including Ca^{2+}, Li^{+}, Mg^{2+}, and PO_4^{3-} (14). These simple signaling ions instruct stem cell differentiation; thus, this scaffold is designed to be intrinsically osteoinductive and degradable while offering mechanical stability derived from the strength of graphene.

Results and Discussion

Synthetic Incorporation of Inducerons. We developed a universal synthetic procedure to covalently tether polyphosphates onto GO with an array of counterions, generating PG materials (Scheme 1 and *SI Appendix*, Fig. S1*A*). The addition of a Lewis acid catalyst (15–17) enables the Arbuzov reaction to be applied universally to GO to provide PGs with a controlled density of polyphosphate anchor points and a plethora of counterions. This key addition of magnesium bromide diethyl etherate as a catalyst to activate the epoxides on GO enhances efficiency and enables this functionalization method to serve in biomedical applications: control of the polyphosphate density and incorporation of a wide range of counterions were not previously accessible (18) (*SI Appendix*, Fig. S2). Ca^{2+}, Li^{+}, and Mg^{2+} were incorporated as phosphate counterions for their known osteoinductive capabilities, producing CaPG, LiPG, and MgPG, respectively. K^{+} and Na^{+} were incorporated as non-osteogenic controls, producing KPG and NaPG, respectively.

Characterization of PGs demonstrated effective covalent functionalization with phosphate groups. Deconvolution of both the FTIR spectroscopy (19, 20) and the X-ray photoelectron spectroscopy (XPS) (21, 22) spectra reveals unique peaks corresponding to P–C bonds (Fig. 1 and *SI Appendix*, Figs. S3–S8 and Table S1). Additional characterization using thermogravimetric analysis (TGA) and X-ray diffraction (XRD) demonstrated reduction of the graphenic backbone during functionalization, which should translate to a scaffold with lower oxidative stress and increased compatibility in vivo (23) (*SI Appendix*, Figs. S9 and S10).

Processing into 3D Scaffolds with Osteomimetic Mechanical Properties. For applications as a load-bearing bone scaffold, the mechanical properties of the scaffold must approximate native bone for stabilization. Single-layer and bulk graphene-based composites have excellent mechanical properties (8, 24–26); thus, the graphenic component of PG provides mechanical strength. To create a 3D scaffold, PG powders were processed into pellet constructs (*SI Appendix*, Fig. S1*B*) via hot pressing at moderate temperature and high pressure.

Hot press processing did not disrupt the covalent phosphate functionalization of PG materials. Compared with unprocessed PG powders, PG pellets showed minimal changes in their TGA thermograms as well as their spectra from XPS, Raman spectroscopy, and FTIR spectroscopy (*SI Appendix*, Figs. S3–S9 and S11). TGA confirmed that the processing temperature did not exceed

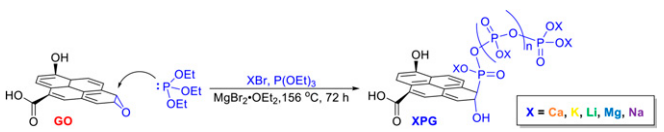

Scheme 1. Development of a catalyzed Arbuzov synthesis of PGs with control of the counterions through the ring opening of epoxides on GO. Note that the structure of GO is simplified for clarity.

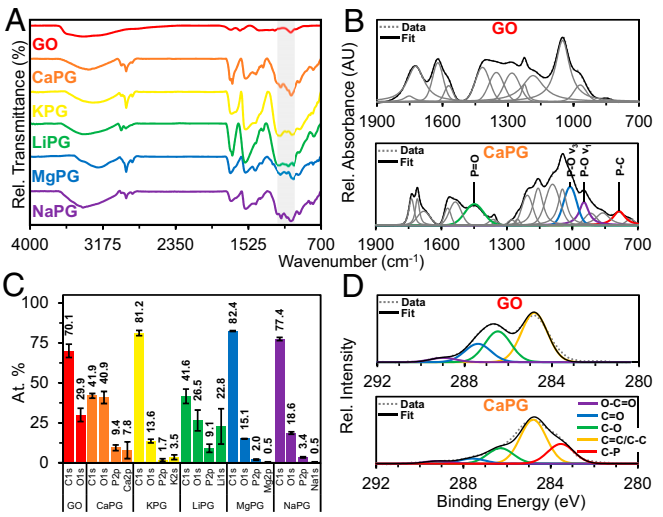

Fig. 1. Chemical characterization of the phosphate functionalization of GO powders. (*A*) FTIR spectra showing the emergence of phosphate stretches between 1,200 and 1,000 cm^{-1} as highlighted in gray. (*B*) Peak deconvolution of FTIR fingerprint regions demonstrating phosphate peaks unique to PG materials, where the presence of the P–C peak is indicative of covalent phosphate functionalization on the graphene backbone. (*C*) XPS elemental analysis of PG materials showing the presence of phosphorus and the respective counterion. (*D*) High-resolution XPS carbon scans demonstrating a P–C stretch at 283.5 eV.

the onset temperature (T_o) of PG powders. XRD indicated a reduction in the intergallery spacing postprocessing that is likely a result of packing from high-pressure processing (*SI Appendix*, Fig. S10).

Compressive universal testing and dynamic mechanical analysis were used confirm that the mechanical properties of PG scaffolds approximated those of bone. With the increased agility of the synthetic method, we were able to tune the chemical functionalization density to the properties of PG scaffolds to exhibit stiffness and strengths comparable with those of bone (27, 28): Young's moduli (E) up to 1.8 GPa, compressive storage moduli (E') up to 291 MPa, shear storage moduli (G') up to 545 MPa, and ultimate compressive strengths (UCS) up to 300 MPa (Fig. 2 and *SI Appendix*, Fig. S12). PG pellets were also tough (U_T; up to 2,326 $J{\cdot}m^{-3}{\cdot}10^4$). Furthermore, the compressive mechanical properties did not display a strain rate dependence (*SI Appendix*, Fig. S13), indicating that the scaffolds could withstand an array of loads associated with activities, such as walking and running, without compromising mechanical integrity. Critically, producing PG scaffolds with biomimetic mechanical properties will prevent stress shielding observed with metallic implants while providing support capable of withstanding large loads to protect the fragile healing interface.

Aqueous Stability of PG Scaffolds. For application in vivo, the 3D PG scaffolds must maintain mechanical integrity in aqueous environments while bone is regenerated. In nonunion bone defects, it is expected that stabilization will be required over the course of a month. Thus, the compressive mechanical properties of pellets in aqueous conditions were evaluated over 28 d (*SI Appendix*, Fig. S14). PG scaffolds remained intact throughout the course of the experiment, except for LiPG, which lost mechanical integrity upon immersion in water. This is likely because the large intergallery spacing enabled water infiltration, accelerating disassembly of LiPG scaffolds. Hydrated PG scaffolds had E' an order of magnitude lower than dry pellets; however, over 28 d in water, minimal changes were observed. In contrast, without the entanglement of the polyphosphate chains, GO pellets were unstable and rapidly dispersed in water (*SI Appendix*, Fig. S1*C*).

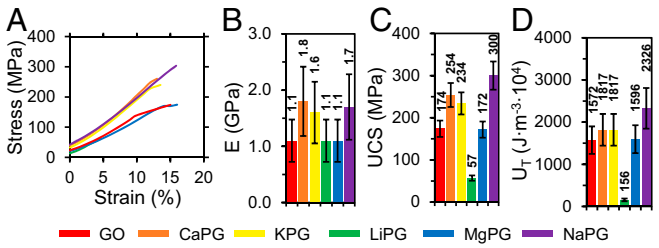

Fig. 2. Mechanical characterization of the PG scaffolds. (*A*) Compressive universal testing until failure at a 0.1-s^{-1} strain rate, (*B*) Young's moduli (*E*), (*C*) *UCS*, and (*D*) toughness (U_T) of graphenic constructs. All data were calculated from the stress–strain curves; $n = 3$. Bars and the listed values are sample means, and error bars are sample SDs.

FTIR, TGA, and XPS analyses of scaffolds after prolonged aqueous exposure revealed that the CaPG scaffold underwent significant chemical changes into a structure resembling reduced GO (*SI Appendix*, Figs. S3–S9). We consider this result to be especially promising, as it suggests that CaPG shares an aqueous degradation pathway with GO and that the large volume of literature studying the compatibility of GO is indicative of the compatibility of CaPG. Additional experiments are underway to confirm this hypothesis.

Elution of Inducerons. We hypothesized that, over the course of degradation, CaPG scaffolds were eluting osteoinductive Ca^{2+} and PO_4^{3-} ions during their aqueous degradation. We were able to quantitatively measure Ca^{2+} elution (29) from CaPG scaffolds in PBS, revealing a controlled delivery of up to 500 μM of Ca^{2+} per 1 mg of CaPG (*SI Appendix*, Figs. S15 and S16). The release profile of Ca^{2+} showed an initial burst release within the first day followed by a controlled release up to day 14. The final Ca^{2+} concentration was ∼10 mM, which is similar to the ideal concentration of ∼8 mM for osteogenic differentiation (30). After fitting the data to a mathematical model (31), we concluded that the elution of Ca^{2+} was diffusion controlled. Furthermore, PO_4^{3-} was also released from CaPG pellets with a burst release profile that reached equilibrium after the second day (*SI Appendix*, Figs. S15 and S16). CaPG scaffolds deliver up to 20 μM of PO_4^{3-} per 1 mg of CaPG. Since Ca^{2+} and PO_4^{3-} are known to induce osteogenic differentiation, this suggests that a degradable CaPG scaffold is a highly promising material for controlled release of inducerons to support osteogenic differentiation.

Compatibility and Osteoconductivity in Vitro. We prepared and characterized aqueous dispersions of PG materials and demonstrated that they are cytocompatible and did not alter subcellular compartments using NIH-3T3 fibroblasts, RAW 264.7 macrophages, and human mesenchymal stem cells (hMSCs) (*SI Appendix*, Figs. S17–S20) (32). Cells adhere to and grow on PG substrates (*SI Appendix*, Fig. S19) and pellets (Fig. 3), demonstrating osteoconductivity.

Osteoinduction in Vitro. The efficacy of a bone regeneration scaffold can be enhanced if the material promotes osteogenic differentiation of hMSCs. Excitingly, CaPG encourages expression of an osteoblastic phenotype in hMSCs in vitro (Fig. 4). Alkaline phosphatase (ALP) is highly expressed in osteoblasts (33) and is a quantitative stain correlating with the level of osteoblastic expression. hMSCs exposed to CaPG and cultured in growth media (designed to maintain multipotency with no added growth factors) exhibited a 240% increase in ALP expression (Fig. 4 *A* and *D*). Compared with hMSCs cultured in osteogenic media (commercially available media designed to maximize osteogenic differentiation using growth factors), cells exposed to CaPG had similar expression levels. A similar result was obtained when assaying for Alizarin Red S (ARS), which labels calcium deposits that are indicative of mineralization from cells displaying an osteogenic phenotype (34): hMSCs exposed to CaPG had a 170% increase in the intensity of the ARS labeling (Fig. 4 *B* and *E*). Other PGs and GO showed intermediate increases in these levels; however, the ability of CaPG to intrinsically induce osteogenesis to the same extent as growth factors is particularly remarkable.

qRT-PCR was used to quantify the expression of important osteogenic genes of hMSCs exposed to PG materials: collagen type I alpha 1 (*COL1A1*), bone morphogenetic protein 2 (*BMP-2*), and runt-related transcription factor 2 (*RUNX-2*). Small nuclear ribonucleoprotein D3 (*SNRPD3*) and proteasome subunit beta 2 (*PSMB2*) were used as reference genes due to their constant levels of expression (35). Cellular exposure to either PG materials or osteogenic media for 14 d resulted in relatively small changes in the expression of the genes examined compared with the no treatment growth media control (Fig. 4*C*). At this time point, hMSCs were expressing ALP, a phenotypic marker of osteoblasts, indicating that hMSCs were already committed to the osteoblastic lineage. Since it is during the early stages of osteogenic differentiation that the potent growth factor BMP-2 serves to activate *RUNX-2*, which is considered the principle osteogenic master switch (36–38), it is likely that peak expression of these osteogenic genes has already passed. Type I collagen is a target of RUNX-2 (36–38), and optical imaging confirmed that, after 14 d, cells were confluent and already generated a substantial amount of extracellular matrix.

Overall, in vitro, CaPG was best able to induce differentiation of hMSCs into an osteoblastic phenotype. Even in growth media designed to preserve multipotency, CaPG resulted in significant osteogenic differentiation of hMSCs that was similar to that observed for hMSCs cultured in osteogenic media with growth factors tailored to induce osteogenesis. This superior differentiation likely results from controlled release of Ca^{2+} and PO_4^{3-} inducerons, structural mimicry of natural bony apatite, and mechanical stiffness. Thus, CaPG shows promise as a cell-instructive, intrinsically osteoinductive material.

In Vivo Evaluation of Osteoinductivity. To verify the intrinsic osteoinductivity of CaPG in vivo, we studied ectopic bone formation in the s.c. space of mice. We chose this model, because osteoinductivity is clearly observable, while the ability to grow bone in this nonnatural position is more challenging and thus, more indicative of the innate abilities of the material. The experiment compared three materials: (*i*) GO (to determine the baseline osteoinductivity of a generic unmodified material); (*ii*) CaPG (to test the osteoinductivity of this osteomimetic FGM); and (*iii*) GO + recombinant human bone morphogenetic protein 2 (rhBMP-2) as a positive control, as

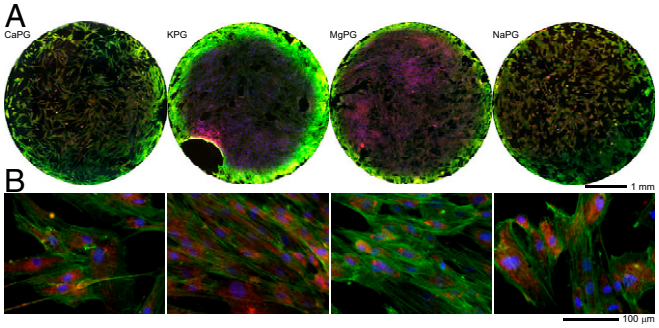

Fig. 3. hMSCs adhere to and grow on 3D scaffolds of PG materials. (*A*) Whole-pellet images (top view) and (*B*) higher-magnification images of hMSCs cultured on PG pellets for 7 d and then labeled for nuclei (blue), F-actin (green), and mitochondria (red).

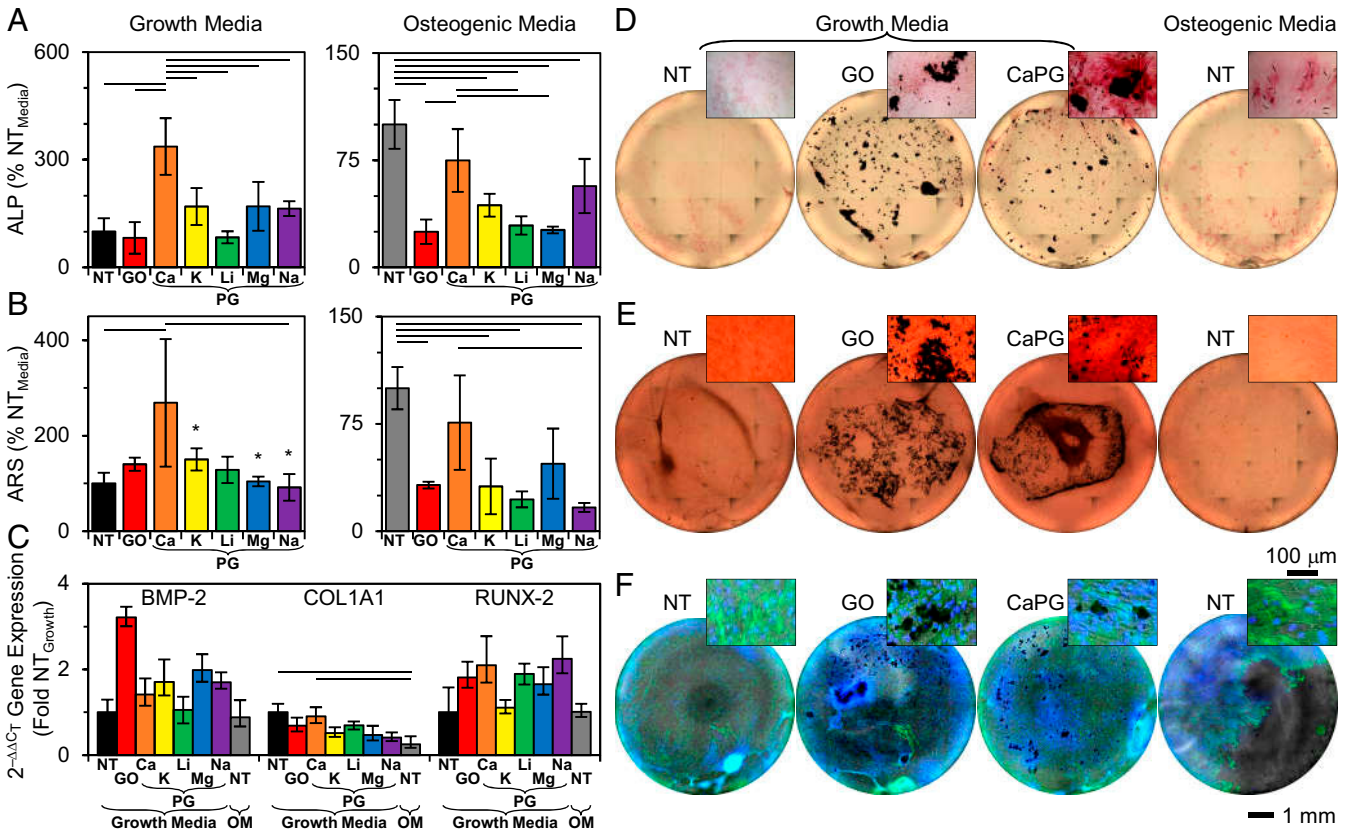

Fig. 4. CaPG induces osteogenic differentiation of hMSCs. (*A*) ALP expression of hMSCs exposed to PG materials for 10 d for growth media and 21 d for osteogenic media. ANOVA *F* values: 13.48 for growth media and 12.83 for osteogenic media. (*B*) ARS of hMSCs exposed to PG materials for 28 d quantified from ARS absorbance. ANOVA *F* value: 3.66 for growth media and 8.44 for osteogenic media. *$n < 3$ due to off-center localization of the majority of hMSCs (*SI Appendix, SI Text*). (*C*) Gene expression after 14 d of exposure to PG materials quantified from qRT-PCR using the $2^{-\Delta\Delta Ct}$ method compared with two reference genes. Note that the no treatment (NT) growth media sample is the calibrator. ANOVA *F* value: 1.88 for *BMP-2*, 3.30 for *COL1A1*, and 1.37 for *RUNX-2*. (*D–F*) Representative whole-well and higher-magnification images of (*D*) ALP expression (red); (*E*) ARS expression (red); and (*F*) nuclei (blue), F-actin (green), and phase contrast (gray). Bars are sample means, and error bars are sample SDs except for *C*, for which they are propagated SEs; $n = 3$ for all except for ALP growth media, for which $n = 4$. Lines between bars indicate a two-tailed *P* value < 0.05 from Sidak post hoc test.

we hypothesized that GO would localize rhBMP-2 to support bone formation. Each material was tested with and without exogenous bone marrow stromal cells (BMSCs).

A transgenic fluorescent reporter mouse model was used to delineate the contribution of host and donor cells in ectopic bone formation (39). Col3.6 fluorescent protein reporter mice contain a 3.6-kb DNA fragment derived from the rat type I collagen (collagen I alpha 1) promoter that directs strong expression of fluorescent protein in preosteoblasts and osteoblasts. Fluorescence intensity reflects levels of osteogenic differentiation, with low levels of expression in osteoprogenitor cells and increasingly higher levels of expression during osteoblast maturation. This combined with histological methods allows for preservation of fluorescence in nondecalcified bone and enables imaging of osteoblast reporters with mineralization fluorochromes and ALP staining. This allows for a determination of cells that are retained on injection and cells that are recruited due to the osteoinductive capacities of the material. To eliminate the effect of processing conditions, FGMs were delivered through injection of an FGM slurry, which coalesced to form a pseudoimplant in vivo. This delivery method has been previously reported (23), and it enables convenient cellular loading onto FGMs and reduces trauma at the implant site (*SI Appendix*, Fig. S21).

Implant sites showed no obvious tissue necrosis or toxicity. At 8 wk postinjection, GO and CaPG implants showed cellular infiltration with evidence of cellular uptake and clearance. Histological sections of liver, spleen, and kidneys showed no obvious tissue damage, toxicological effects, or inflammation. Also, no accumulation of GO or CaPG was observed in any of these tissues (*SI Appendix*, Fig. S22). These observations suggest good long-term compatibility for graphenic implants in vivo.

Innate osteoinductivity has been suggested for GO (40–43), but the effect was minimal under these conditions. Of 10 injections of GO with BMSCs, only 1 showed the presence of cyan donor cells after 8 wk, showing a weak ability of GO to retain donor cells at the implantation site (Fig. 5*C*). Interestingly, the one implant that retained donor cells at the implantation site showed ectopic mineralized tissue formation contributed by both donor and host cells. GO implanted without donor cells showed no osteoinductivity.

CaPG showed significant intrinsic osteoinductivity in vivo when implanted with BMSCs. Of the 10 implants, 4 showed the presence of cyan donor cells 8 wk postimplantation. Bony matrix was confirmed by the presence of white mineralized tissue throughout the implant along with strong alizarin complexone (AC) labeling of calcific depositions and ALP activity (Fig. 5*D*). Analysis of the high-magnification area at a cellular level showed colocalization of bright topaz and cyan fluorescent signals with sharp AC lines and ALP-positive osteoblasts. Tartrate-resistant acid phosphatase (TRAP) is a marker of osteoclasts, and areas of TRAP-positive cells within the implant demonstrate active resorption and remodeling of the implant. CaPG implants that failed to retain BMSCs or were injected without BMSCs failed to

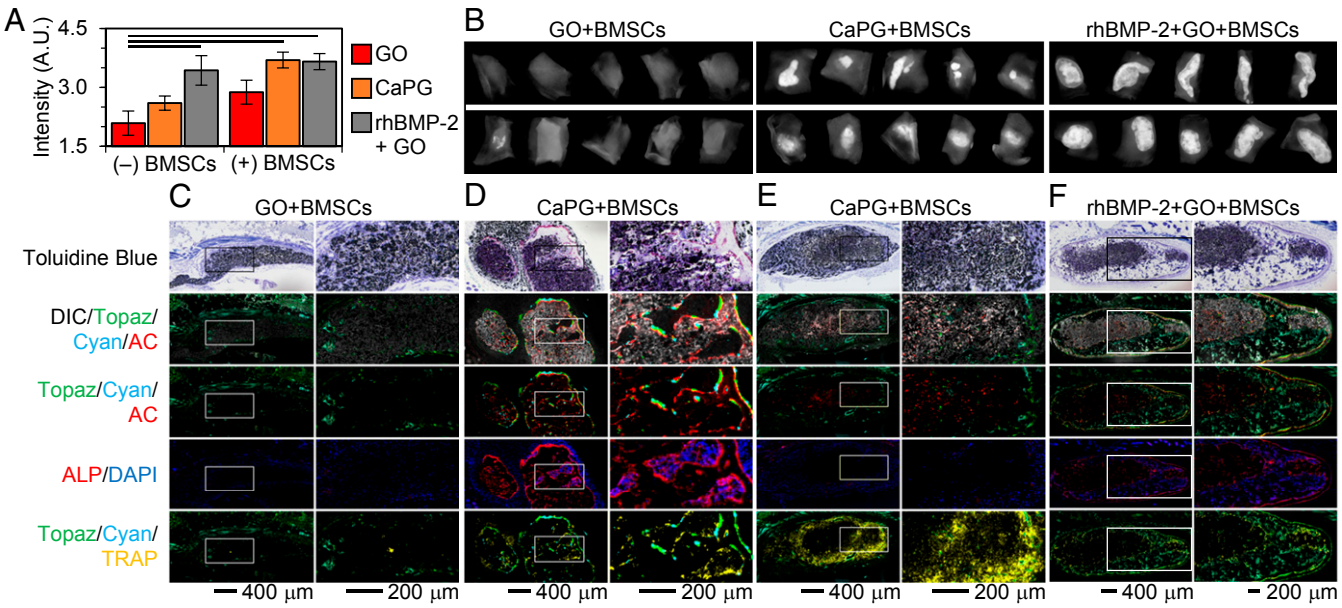

Fig. 5. CaPG in the presence of BMSCs induces osteogenesis in vivo after 8 wk. (*A*) Quantification of X-ray image intensity demonstrates that CaPG significantly increases the formation of mineralized tissue compared with GO. When CaPG was combined with BMSCs, the corresponding X-ray image intensity was statistically similar (*P* value = 1) to that observed for s.c. injections of rhBMP-2. Note that bars are sample means and error bars are SEMs; $n = 10$. ANOVA *F* value: 6.94; lines between bars indicate a two-tailed *P* value < 0.05 from Sidak post hoc test. (*B*) Representative X-ray images of the harvested s.c. tissue. (*C*–*F*) Histology showing toluidine blue and overlay images of differential interference contrast (DIC) (grayscale), donor BMSCs (cyan), host cells (topaz), AC (red), ALP (red), DAPI (blue), and TRAP (yellow). Mineral accumulation is shown in white in DIC images. Host-derived and donor-derived osteoblasts are expressing bright topaz and cyan signals, respectively, that are colocalized with a sharp AC label and ALP staining. The AC label indicates active mineralization in the past 24 h, whereas ALP staining represents ALP-positive osteoblasts. Cell nuclei are stained blue with DAPI. TRAP-positive osteoclasts are identified by their bright yellow stain that is colocalized with faint topaz/cyan cells. Host-derived fibroblasts express faint topaz and are negative for AC, ALP, or TRAP. Undifferentiated donor cells are expressing faint cyan and are negative for AC, ALP, or TRAP.

induce osteogenesis ectopically. These results showed the ability of CaPG to significantly enhance the retention of donor cells and provide signals intrinsically without the use of growth factors to direct osteogenesis.

We also investigated noncovalent modification of GO with rhBMP-2, since rhBMP-2 is a better positive control than demineralized bone matrix in these transgenic mice (44). GO is known to adsorb proteins (45), and excitingly, we found that this association was sufficient to retain rhBMP-2 in a bioactive form at the injection site. The GO + rhBMP-2 implants were enveloped by a uniform and compact mineralized bone tissue resembling cortical bone overlaid with ALP-positive osteoblasts and strong AC label (*SI Appendix*, Fig. S23*D*). There were also areas of trabecular-like bone within the implant that were positive for AC label and ALP activity. The presence of TRAP-positive cells within the implant site implies active tissue resorption and remodeling. Additionally, the implant site showed the presence of ALP-negative nonmineralized compartments, indicating the formation of marrow-like tissue.

The addition of BMSCs to the GO + rhBMP-2 group also led to localized s.c. bone formation similar to that observed in the GO + rhBMP-2 group (Fig. 5*F*). Of the 10 implants, 3 showed the presence of cyan donor cells colocalized with topaz host cells within the mineralized tissue indicating the donor and host cell contribution in bone formation. Quantitative radio opacity measurement, however, did not show significant differences between the GO + rhBMP-2 and GO + rhBMP-2 + BMSC groups, implying that addition of BMSCs to GO + rhBMP-2 did not significantly increase the extent of bone formation. Overall, GO was able to successfully bind and retain rhBMP-2 at the s.c. injection site and support ectopic bone formation in a localized manner.

Summary and Impact

We report the creation of intrinsically osteoinductive scaffolds for bone regeneration composed of FGMs. Using a Lewis acid-catalyzed Arbuzov reaction enables unprecedented control of GO functionalization to produce biomimetic PGs. PGs and specifically, CaPG were shown to elute inducerons, small ions that induce osteogenesis, including Ca^{2+} and PO_4^{3-}, in aqueous conditions. CaPG was shown to induce osteogenesis in vitro to the same extent as growth factors. In vivo, CaPG was found to also be intrinsically osteoinductive when implanted with BMSCs. Also, noncovalent modification of GO with rhBMP-2 showed excellent osteoinductivity in vivo. These findings demonstrate the potential of FGMs as intrinsically osteoinductive scaffolds that support bone regeneration. Additional work is underway to process these materials into customizable scaffolds and to optimize the osteoinductive qualities through synergistic delivery of rhBMP-2 with CaPG. Our FGM scaffolds could change the way that physicians treat severe bone injuries: enabling patients to recover fully through complete regeneration of functional healthy bone.

Methods

All aspects of the animal protocol were approved by UConn Health Institutional Animal Care and Use Committee (IACUC). Full details are provided in *SI Appendix*.

ACKNOWLEDGMENTS. For providing use of their facilitates, we thank K. Matyjaszewski (dynamic light scattering), M. Bruchez (plate reader), N. Washburn (lyophilizer), V. Hinman (qRT-PCR thermocycler), K. Noonan (absorbance spectrophotometer), and K. Whitehead (NIH-3T3 and RAW 264.7 cells) (all at Carnegie Mellon University). We thank J. Gillespie for providing training and use of the XPS (Materials Characterization Laboratory at the University of Pittsburgh) and J. Doloff (Massachusetts Institute of Technology) for useful discussions regarding qRT-PCR. We acknowledge the efforts of A. Moy (Carnegie Mellon University) for XRD and thank D. Rowe (UConn Health) for helpful discussions on the in vivo data. We acknowledge H.-M. Kan, S. Gohil,

L. Nair, Z. Wu, Y. Liu, and X. Xiu for their assistance in the in vivo studies and thank L. Chen for histological support (all at UConn Health). This work was supported by Carnegie Mellon University startup grants (to S.A.S.) and US NIH Director's Pioneer Award DP1-AR-068147 (to C.T.L.). The authors acknowledge use of the Materials Characterization Facility at Carnegie Mellon University, which was supported by Carnegie Mellon University Grant MCF-677785.

1. Ehrenfeld M, Manson PN, Prein J (2012) *Principles of Internal Fixation of the Craniomaxillofacial Skeleton: Trauma and Orthognathic Surgery* (Thieme Medical Publishers, Inc., New York).
2. Albrektsson T, Brånemark PI, Hansson HA, Lindström J (1981) Osseointegrated titanium implants. Requirements for ensuring a long-lasting, direct bone-to-implant anchorage in man. *Acta Orthop Scand* 52:155–170.
3. Langer R, Vacanti JP (1993) Tissue engineering. *Science* 260:920–926.
4. Holmes D (2017) Closing the gap. *Nature* 550:S194–S195.
5. Sánchez Alvarado A, Yamanaka S (2014) Rethinking differentiation: Stem cells, regeneration, and plasticity. *Cell* 157:110–119.
6. Watt FM, Driskell RR (2010) The therapeutic potential of stem cells. *Philos Trans R Soc Lond B Biol Sci* 365:155–163.
7. Morrison SJ, Spradling AC (2008) Stem cells and niches: Mechanisms that promote stem cell maintenance throughout life. *Cell* 132:598–611.
8. Suk JW, Piner RD, An J, Ruoff RS (2010) Mechanical properties of monolayer graphene oxide. *ACS Nano* 4:6557–6564.
9. Dimiev AM, Alemany LB, Tour JM (2013) Graphene oxide. Origin of acidity, its instability in water, and a new dynamic structural model. *ACS Nano* 7:576–588.
10. Kostarelos K, Novoselov KS (2014) Materials science. Exploring the interface of graphene and biology. *Science* 344:261–263.
11. Holt BD, Arnold AM, Sydlik SA (2016) In it for the long haul: The cytocompatibility of aged graphene oxide and its degradation products. *Adv Healthc Mater* 5:3056–3066.
12. Eigler S, Hirsch A (2014) Chemistry with graphene and graphene oxide-challenges for synthetic chemists. *Angew Chem Int Ed Engl* 53:7720–7738.
13. Cushnie EK, et al. (2014) Simple signaling molecules for inductive bone regenerative engineering. *PLoS One* 9:e101627.
14. O'Neill E, Awale G, Daneshmandi L, Umerah O, Lo KW-H (2018) The roles of ions on bone regeneration. *Drug Discov Today* 23:879–890.
15. Renard P-Y, Vayron P, Leclerc E, Valleix A, Mioskowski C (2003) Lewis acid catalyzed room-temperature Michaelis-Arbuzov rearrangement. *Angew Chem Int Ed Engl* 42: 2389–2392.
16. Rajeshwaran GG, Nandakumar M, Sureshbabu R, Mohanakrishnan AK (2011) Lewis acid-mediated Michaelis-Arbuzov reaction at room temperature: A facile preparation of arylmethyl/heteroarylmethyl phosphonates. *Org Lett* 13:1270–1273.
17. Subramanyam C, et al. (2015) Bismuth(III) chloride mediated Michaelis–Arbuzov reaction: A facile synthesis of substituted arylphosphonates/phosphinates and bioactivity evaluation. *Phosphorus Sulfur Silicon Relat Elem* 190:1948–1957.
18. Goods JB, Sydlik SA, Walish JJ, Swager TM (2014) Phosphate functionalized graphene with tunable mechanical properties. *Adv Mater* 26:718–723.
19. Larkin P (2017) *Infrared and Raman Spectroscopy: Principles and Spectral Interpretation* (Elsevier, Cambridge, MA).
20. Coates J (2006) Interpretation of infrared spectra, a practical approach. *Encyclopedia of Analytical Chemistry*, ed Myers RA (Wiley, Chichester, UK), pp 10881–10882.
21. Sun J, et al. (2014) Formation of stable phosphorus-carbon bond for enhanced performance in black phosphorus nanoparticle-graphite composite battery anodes. *Nano Lett* 14:4573–4580.
22. Liu Y, et al. (2017) Red phosphorus nanodots on reduced graphene oxide as a flexible and ultra-fast anode for sodium-ion batteries. *ACS Nano* 11:5530–5537.
23. Sydlik SA, Jhunjhunwala S, Webber MJ, Anderson DG, Langer R (2015) In vivo compatibility of graphene oxide with differing oxidation states. *ACS Nano* 9:3866–3874.
24. Chen C, et al. (2009) Performance of monolayer graphene nanomechanical resonators with electrical readout. *Nat Nanotechnol* 4:861–867.
25. Gong T, et al. (2015) Thickness dependence of the mechanical properties of free-standing graphene oxide papers. *Adv Funct Mater* 25:3756–3763.
26. Gao Y, et al. (2011) The effect of interlayer adhesion on the mechanical behaviors of macroscopic graphene oxide papers. *ACS Nano* 5:2134–2141.
27. Kutz M (2003) Standard handbook of biomedical engineering & design. Available at https://www.accessengineeringlibrary.com/browse/standard-handbook-of-biomedical-engineering-and-design. Accessed December 10, 2017.
28. Henkel J, et al. (2013) Bone regeneration based on tissue engineering conceptions: A 21st century perspective. *Bone Res* 1:216–248.
29. Spectrum Diagnostics (2018) Calcium O-CPC (2011) Available at www.spectrum-diagnostics.com/new/pdf/01_Clinical_Chemistry/03_Electrolytes/Calcium%20O-CPC.pdf. Accessed December 21, 2016.
30. Chai YC, Roberts SJ, Schrooten J, Luyten FP (2011) Probing the osteoinductive effect of calcium phosphate by using an in vitro biomimetic model. *Tissue Eng Part A* 17: 1083–1097.
31. Dash S, Murthy PN, Nath L, Chowdhury P (2010) Kinetic modeling on drug release from controlled drug delivery systems. *Acta Pol Pharm* 67:217–223.
32. Caplan AI (1991) Mesenchymal stem cells. *J Orthop Res* 9:641–650.
33. Golub EE, Boesze-Battaglia K (2007) The role of alkaline phosphatase in mineralization. *Curr Opin Orthop* 18:444–448.
34. Puchtler H, Meloan SN, Terry MS (1969) On the history and mechanism of alizarin and alizarin red S stains for calcium. *J Histochem Cytochem* 17:110–124.
35. Eisenberg E, Levanon EY (2013) Human housekeeping genes, revisited. *Trends Genet* 29:569–574.
36. Knippenberg M, Helder MN, de Blieck-Hogervorst JM, Wuisman PI, Klein-Nulend J (2007) Prostaglandins differentially affect osteogenic differentiation of human adipose tissue-derived mesenchymal stem cells. *Tissue Eng* 13:2495–2503.
37. Patil S, Paul S (2014) A comprehensive review on the role of various materials in the osteogenic differentiation of mesenchymal stem cells with a special focus on the association of heat shock proteins and nanoparticles. *Cells Tissues Organs* 199:81–102.
38. Marie PJ, Fromigué O (2006) Osteogenic differentiation of human marrow-derived mesenchymal stem cells. *Regener Med* 1:539–548.
39. Kalajzic I, et al. (2002) Use of type I collagen green fluorescent protein transgenes to identify subpopulations of cells at different stages of the osteoblast lineage. *J Bone Miner Res* 17:15–25.
40. Shadjou N, Hasanzadeh M (2016) Graphene and its nanostructure derivatives for use in bone tissue engineering: Recent advances. *J Biomed Mater Res A* 104:1250–1275.
41. Li M, et al. (2018) An overview of graphene-based hydroxyapatite composites for orthopedic applications. *Bioact Mater* 3:1–18.
42. Dubey N, et al. (2015) Graphene: A versatile carbon-based material for bone tissue engineering. *Stem Cells Int* 2015:804213.
43. Holt BD, Wright ZM, Arnold AM, Sydlik SA (2016) Graphene oxide as a scaffold for bone regeneration. *Wiley Interdiscip Rev Nanomed Nanobiotechnol* 9:e1437.
44. Alaee F, et al. (2014) Evaluation of osteogenic cell differentiation in response to bone morphogenetic protein or demineralized bone matrix in a critical sized defect model using GFP reporter mice. *J Orthop Res* 32:1120–1128.
45. Georgakilas V, et al. (2016) Noncovalent functionalization of graphene and graphene oxide for energy materials, biosensing, catalytic, and biomedical applications. *Chem Rev* 116:5464–5519.